International Journal of Hydrogen Energy, Vol. 2, pp. 139–153. Pergamon Press, 1977. Printed in Northern Ireland

HEAT AND MASS TRANSFER ANALYSIS OF BACON-TYPE HYDROGEN–OXYGEN FUEL CELLS: THE VOLUME AVERAGE VELOCITY

Y. BAYAZITOGLU

Department of Mechanical Engineering, University of Houston, Houston, Texas 77004, U.S.A.

and

G. E. SMITH

Department of Mechanical Engineering, University of Michigan, Ann Arbor, Michigan 48104, U.S.A.

Abstract—A model is developed to study the transient electrolyte water evaporation and heat rejection in an operating fuel cell. The model applies to fuel cells which circulate reactant gas in excess of that consumed in the electrochemical reaction to remove the product water as well as heat.

The model mass transfer equations are expressed in terms of volume average velocity. It has been shown that the mathematical representation of the volume average velocity model is attractive for computational purposes, since the volumetric disappearance of electrolyte volume for a fixed control volume in space would yield a change in concentration as would actually occur due to dilution.

Because of the non-linearities associated with the developed model equations, the finite-difference technique is used to obtain solutions. The implicit finite-difference scheme was selected so as to avoid the stability criteria associated with the explicit form, which places an undesirable restriction on the size of the time increment that can be used. After its accuracy had been established, the method was used to study an operating Bacon-type Hydrogen–oxygen fuel cell.

NOMENCLATURE

A	a constant;
B	a constant;
D	diffusivity;
F	Faraday's constant;
F_1	concentration of KOH by weight;
i	current density;
m	mass flux;
m_1	mass of KOH;
M	molecular weight;
P	electrode fine pore porosity;
P_e	partial pressure of water in electrolyte;
P_{eff}	electrode porosity;
P_s	partial pressure of water in hydrogen gas chamber;
q	deformation velocity;
R	universal gas constant;
r_2	electrode fine pore radius;
S	area;
t	time;
t_e	distance between electrodes;
t_g	thickness of electrode;
t_h	hydrogen chamber thickness;
t_0	oxygen chamber thickness;
T	temperature;
v	volume average velocity;
V	volume;
$\bar{V}$	partial molal volume;
W	width of electrode;
W_1	humidity ratio;
z	valence of ions;
Z	height of electrode;

Greek Letters

ρ	density;
τ	temperature;
φ_{soln}	electrical potential;

Subscripts

a anode;
c cathode
1 KOH
2 H_2O

Superscripts

− OH^-
+ K^+

INTRODUCTION

It is the purpose of this study to combine appropriate heat, mass and electrochemical disciplines to develop a mathematical model and the associated digital computer simulation such that the operating conditions of a fuel cell can be determined. The model presented in this study is developed for only single cells.

The by-products of the electrochemical reaction in the hydrogen–oxygen fuel cell are heat and water. These products must be removed from the cell to avoid exceeding the maximum critical temperature of the cell and to prevent an excessive increase in electrolyte volume and decrease in electrolyte concentration, any one of which can cause failure or malfunction of the cell. In addition, removal of heat and water at a controlled rate provides an effective means of maintaining the cell operating conditions within the design range. One technique of removing water as well as heat from a hydrogen–oxygen fuel cell is to circulate hydrogen in excess of that consumed in the electrochemical reaction. Since the aim in fuel technology is to develop highly reliable, long life, high performance fuel cell systems, the design of systems needed to achieve this type of control could be greatly aided by an understanding of the mechanisms that regulate the transport and hence the rejection of the heat and water produced in an operating cell as discussed in [1] and [2].

An experimental and analytical study of the dynamics of water rejection in a Bacon-type hydrogen–oxygen fuel cell was conducted by Prokopius and Hagedorn [3]. The module tested was constructed of 15 cells electrically connected in series. These cells were operated near 204°C and at atmospheric pressure, with an aqueous potassium hydroxide electrolyte about 75% KOH by weight contained between dual-porosity electrodes. A mathematical model was constructed as part of the study which considered the water rejection process from an isothermal hydrogen–oxygen fuel cell with a lumped parameter treatment of the conservation of mass of water in the electrolyte. A mathematical model was developed at the NASA Lewis Research Center that simulates the transport in both Bacon and alkaline-matrix cells by Prokopius and Easter [4]. The model equations were simulated on an analog computer, and the thermal effects were accounted for by superimposing the temperature correction on the program-calculated vapor pressure. For any particular perturbation, experimental data on cell-temperature response were used to obtain a corresponding correction in vapor pressure of the electrolyte.

Reference [3] and [4] studied the change in electrolyte concentration by using a lumped parameter mass transport analysis. The effect of a distributed electrolyte concentration profile is included in the study reported herein by combining the mass transport and charge transport equations and by expressing these equations in terms of volume average velocity.

ANALYSIS

Deformation and flow

Consider an arbitrary volume $V(t)$, bounded by a surface $S(t)$ as shown in Fig. 1. If a continuous medium of density ρ fills the volume at time t, from the conservation of mass the rate of increase in the total mass in the volume will be equal to the amount of mass flowing through $S(t)$,

$$\frac{\mathrm{d}}{\mathrm{d}t}\int_{V(t)} \rho \, \mathrm{d}V(t) = -\int_{S(t)} \hat{n} \cdot \mathbf{m} \, \mathrm{d}S(t), \tag{1}$$

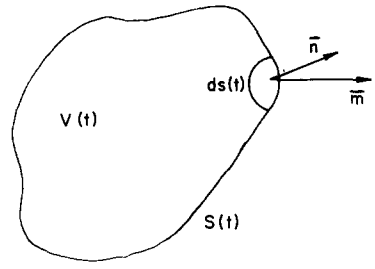

FIG. 1. Arbitrary volume $V(t)$.

where $\hat{n}$ is the unit normal to the area dS, $\hat{n} \cdot \mathbf{m}$ is the normal component of mass flux vector per unit area through dS.

If the coordinates are regarded as curvilinear coordinates in the deformed configuration, the deformed volume element of the reference state $dV_0(t=0)$, due to Euler [5] is

$$dV = |J|\, dV_0, \tag{2}$$

where $|J|$ is the absolute value of the Jacobian determinant; the determinant of the deformation-gradient matrix referred to the reference state.

The relation between the deformed infinitesimal area dS and this area in the reference state as reported by NANSON [5] is,

$$\hat{n}\, dS = |J|\, \hat{N} \cdot F^{-1}\, dS_0, \tag{3}$$

where $\hat{N}$ is the unit normal to the area dS_0, F^{-1} is the inverse of the deformation-gradient matrix.

The infinitesimal volume Eq. (2) and the infinitesimal area Eq. (3) may be substituted into Eq. (1). Both ρ and $\mathbf{m}$ are continuous through V_0 and S_0 and the divergence theorem may be applied to the right hand side to get

$$\int_{V_0} \frac{d}{dt}(\rho\,|J|)\, dV_0 = -\int_{V_0} \nabla \cdot (|J|\, F^{-1} \cdot \mathbf{m})\, dV_0. \tag{4}$$

To obtain the left-hand side of Eq. (4) from (1), it may be noted that the operations of integration with respect to volume and differentiation with respect to time can be performed in reverse order because V_0 is independent of time and the integrand is continuous for any volume V. Since the integral of (4) vanishes for an arbitrary choice of volume, it follows that the integrand must vanish at each point of a region in which no mass is created or destroyed.

$$\frac{d}{dt}(\rho\,|J|) = -\nabla(|J|\, F^{-1} \cdot \boldsymbol{m}). \tag{5}$$

Defining $\mathbf{q}$ as the deformation velocity, we obtain Eq. (5) in terms of spatial coordinates, namely

$$\frac{d\rho}{\partial t} + \boldsymbol{q} \cdot \nabla\rho + \rho\nabla \cdot \mathbf{q} = -\nabla \cdot (F^{-1} \cdot \mathbf{m}). \tag{6}$$

The conservation of volume for this arbitrary volume $V(t)$ in curvilinear coordinate may be expressed as

$$\frac{d}{dt}\int_{V(t)} dV(t) = -\int_{S(t)} \hat{n} \cdot \mathbf{V}\, dS(t), \tag{7}$$

where $\hat{n} \cdot \mathbf{V}$ is the normal component of the volume flux vector per unit area through $dS(t)$. Similarily, Eq. (7) in terms of spatial coordinates, in addition, can be written with d/dt moved

inside the integral to become $\partial/\partial t$ or

$$\frac{\partial |J|}{\partial t} = -\nabla \cdot (|J| F^{-1} \cdot \mathbf{v}). \tag{8}$$

The model

A schematic diagram of the hydrogen–oxygen fuel cell model considered herein is shown in Fig. 2. Hydrogen gas is transported through the porous hydrogen electrode where it is in contact with electrolyte. Hydrogen absorbs on a catalyst embedded in the anode and reacts with hydroxyl ions from the electrolyte to form water and produce electrons which pass through the external circuit to the cathode where they combine with oxygen which is absorbed on a catalyst, and water in the electrolyte to form hydroxyl ions. Migrating of the ions from the cathode through the electrolyte to the anode completes the circuit.

Under transient operating conditions of the cell, the mass of the water will change in the electrolyte (Fig. 3a). This gain or loss of water in the electrolyte will result in changes in the electrolyte concentration in the volume of the electrolyte. Changes in the volume of the electrolyte may be in either the y-direction or the x-direction or in both depending upon the rigidity of the electrolyte cavity. Conservation of mass in spatial coordinates for this case can be developed (Fig. 3c) by considering the change in the electrolyte volume in only the x-direction.

We will first investigate the right hand side of Eq. (6) for each species. Since the mechanism of mass and charge transport are related phenomena, the mass flux of each species in the y-direction in terms of volume average velocity, v, may be written as

$$m^- = J_\phi^- + J^- + \rho^- v \tag{9}$$

$$m^+ = J_\phi^+ + J^+ + \rho^+ v \tag{10}$$

where superscripts $-$ and $+$ denotes OH^- and K^+ ions respectively, ρ is the density and m is the mass flux. The three terms on the right-hand side of (9) and (10) are generally called migration (motion of charged species in an electrical field), diffusion and bulk flow. Attention may now be

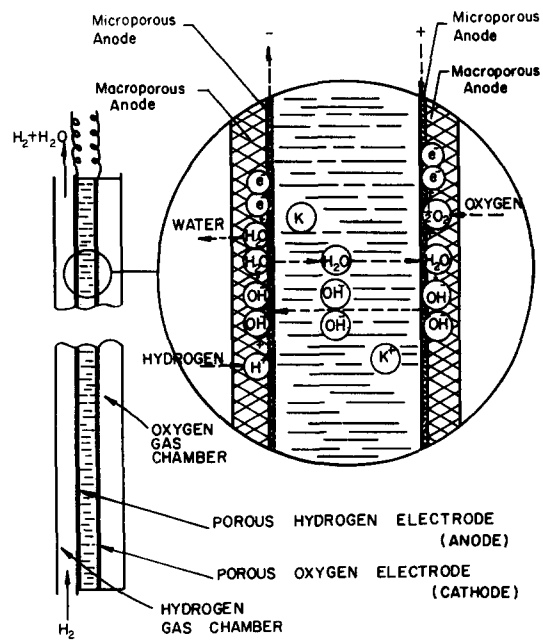

FIG. 2. General mode of operation of a H_2–O_2 fuel cell.

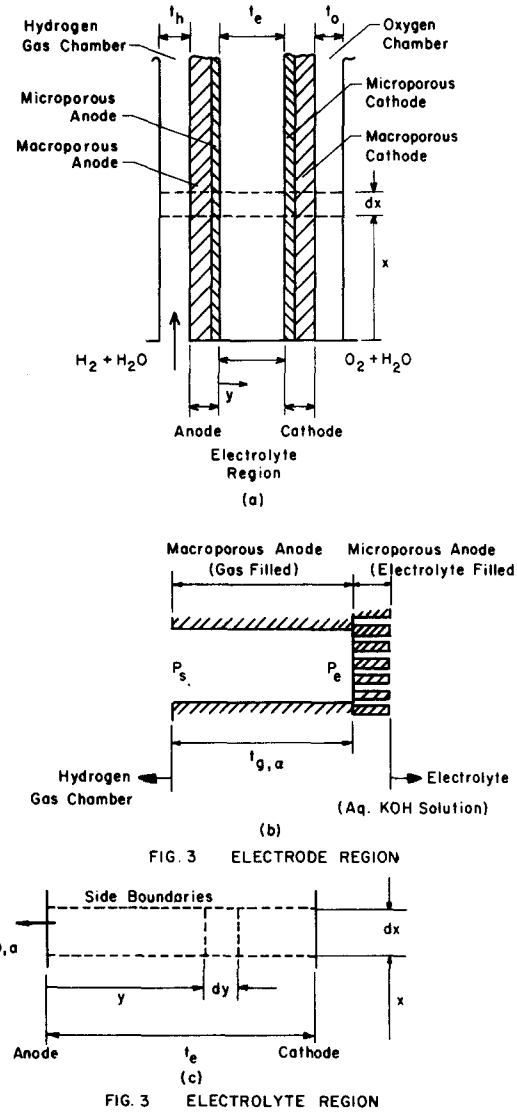

FIG. 3. (a) General features of the system. (b) Electrode region. (c) Electrolyte region

focused on the right-hand side of Eq. (6). Since the change in the volume of the electrolyte is only in the x-direction and the mass flux of species are in the y-direction, the conservation of mass of ions can be developed by using the definitions of mobilities of OH^- and K^+ by the Nernst–Einstein equation assuming a constant diffusion coefficient in water, as follows

$$\frac{\partial \rho^-}{\partial t} + q\frac{\partial \rho^-}{\partial x} + \rho^- \frac{\partial q}{\partial x} = D^-\left[\frac{\partial^2 \rho^-}{\partial y^2} + \frac{z^- F}{\bar{R}T}\frac{\partial}{\partial y}\left(\rho^- \frac{\partial \phi_{soln}}{\partial y}\right)\right] - \frac{\partial}{\partial y}(\rho^- v) \tag{11}$$

$$\frac{\partial \rho^+}{\partial t} + q\frac{\partial \rho^+}{\partial x} + \rho^+ \frac{\partial q}{\partial x} = D^+\left[\frac{\partial^2 \rho^+}{\partial y^2} + \frac{z^+ F}{\bar{R}T}\frac{\partial}{\partial y}\left(\rho^+ \frac{\phi_{soln}}{\partial y}\right)\right] - \frac{\partial}{\partial y}(\rho^+ v), \tag{12}$$

where q is the deformation velocity in the x-direction, D^- and D^+ are the diffusivities in water, z^-, and z^+ are the valence of each ion, ϕ_{soln} is the electrical potential, $\bar{R}$ is the gas constant, T is the temperature and F is Faraday's constant.

The flux of OH^- and K^+ ions constitutes an electrical current, thus the current density, i, is expressed as

$$i = F\left(\frac{z^-}{M^-} m^- + \frac{z^+}{M^+} m^+\right), \tag{13}$$

where M^- and M^+ are the molecular weights.

Since $z^+ = -z^- = 1$, the condition for electroneutrality, Eqs. (11), (12) and (13) can be combined to eliminate the potential terms in (11) and (12). Summing the resultant equations yields

$$\frac{\partial \rho_1}{\partial t} + q\frac{\partial \rho_1}{\partial x} + \rho_1 \frac{\partial q}{\partial x} = D_1 \frac{\partial^2 \rho_1}{\partial y^2} - \frac{\partial}{\partial y}(\rho_1 v), \tag{14}$$

where subscript 1 denotes the KOH specie and $\rho_1 = \rho^- + \rho^+$ and $D_1 = (2D^+D^-/D^+ + D^-)$ [6].

In developing the mass balance equations, it is convenient to use volume average velocity in contrast to using molar or mass average velocities, since during the process the concentration and the density of the solution change but the partial molar volumes can be assumed to be nearly constant. Now we shall use Eq. (8) for this particular application which will yield (Fig. 3c)

$$\frac{\partial q}{\partial x} = -\frac{\partial v}{\partial y}. \tag{15}$$

Next by substituting (15) into Eq. (14) the deformation velocity term in the x-direction can be eliminated. In addition, because of the order of magnitudes of the density gradients the term $q(\partial \rho_1/\partial x)$ compared to the term $v(\partial \rho_1/\partial y)$ can be neglected to obtain

$$\frac{\partial \rho_1}{\partial t} = D_1 \frac{\partial^2 \rho_1}{\partial y^2} - v\frac{\partial \rho_1}{\partial y}. \tag{16}$$

It should be noted that in the present model the volume of the electrolyte can be kept constant in both directions. The volumetric rate of disappearance of electrolyte volume at a point due to volume increase would be $-(\partial v/\partial y)$ and $-\rho_1(\partial v/\partial y)$ will represent the local KOH mass flow out from the side boundaries of the fixed, differential control volume. This will lead to a change in concentration between the electrodes as would actually occur to dilution. In order to find a solution to the above equation a volume average velocity which satisfies the boundary conditions must be chosen. Equation (16) gives the KOH density distribution (ρ_1), and the H_2O density distribution (ρ_2) may be found by the use of conservation of local volume,

$$\rho_1 \frac{\bar{V}_1}{M_1} + \rho_2 \frac{\bar{V}_2}{M_2} = 1, \tag{17}$$

where subscript 2 denotes H_2O and $\bar{V}_1$ and $\bar{V}_2$ are the partial molal volumes in the electrolyte [7] and M_1 and M_2 are the molecular weights.

For the fuel cell operating in a steady-state condition, 1 mole of water is rejected at the hydrogen electrode for each mole of hydrogen consumed by the reaction. Since the molar fluxes of water vapor and hydrogen are equal to each other and are in opposite directions, at steady state the mass transfer is defined as being an equal molar-counter flow diffusion process. For binary gas mixtures at low pressures, at constant pressure and temperature across the electrode, the binary mass diffusivity is nearly independent of mixture composition with the maximum

variation being less than 10% even for extremely different gases [8]. Assuming a constant molar concentration of the mixture over the thickness of the macropore region of the anode [9], at steady state the mass transport of water vapor represented by the proper form of Fick's law is (Fig. 3b).

$$\dot{m}_{\text{evaporated}} = \frac{P_{\text{eff}} D_{2-H} M_2}{RT} \frac{(P_e - P_s)}{t_{g,a}}, \tag{18}$$

where P_{eff} is the effective electrode porosity, D_{2-H} is the diffusivity of water vapor–hydrogen mixture, R is the universal gas constant, T is the temperature of the mixture, P_e is the partial pressure of water in aqueous KOH solution [10]. P_s is the partial pressure of water in the hydrogen gas chamber, $t_{g,a}$ is the thickness of the electrode. This equation will also be applicable during the transients, because at low temperature, fuel cells will have a dilute mixture of hydrogen and water vapor mixture.

The model is described in Fig. 4a. The cell is assumed to be insulated at the two ends in the x-direction, and at the two sides in the y-direction. Figure 4b shows the lumped temperature distributions at various parts of the cell. In developing the equations representing the heat transfer phenomena taking place in the porous electrodes and electrolyte, the temperature distribution in the y-direction is assumed to be uniform based on previous analysis [1]. The heat generated by the irreversibility of the reactions, under current drain, for Bacon-type microelectrodes is calculated by adopting the polarization of the electrodes represented in [5, 11]. Previous analysis [1] has indicated that heats of solution/dilution are negligible for the range of electrolyte concentrations encountered in normal fuel cell operation. Thus they are neglected in the heat generation calculations. A differential slice of the adopted simple pore model is shown in Fig. 5 [12]. It represents the porous media as a number of uniform, parallel cylindrical pores. If the

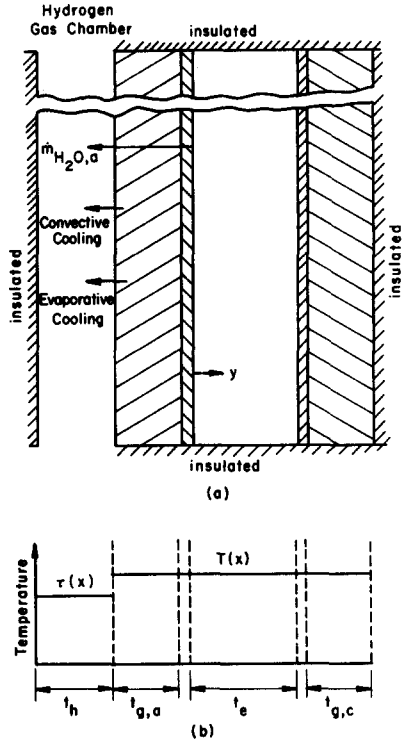

FIG. 4. (a) Model description. (b) Assumed temperature distribution of the model.

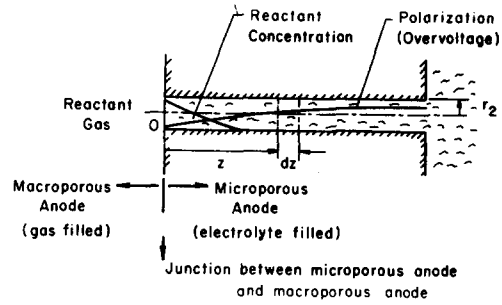

FIG. 5. Simple pore model (micropore)

current is turned off or the cell is operated at a much lower current density than it is designed for, the condensation or evaporation heat effects would primarily involve that for concentration of the electrolyte. Therefore, the differential heat of vaporization of the solvent of the electrolyte should be used for these transients instead of heat of vaporization of pure water [13]. The convective heat transfer coefficient in the gas chamber is represented by the empirical equation in [14].

Because of the non-linearities associated with the developed model equations, the finite difference technique is used to solve the above equations. The implicit form of the difference equations are applied so as to avoid the stability criteria associated with the explicit form, which places an undesirable restriction on the size of the time increment which can be used. Some of the data required in the computer program is obtained by using a subroutine which performs a search of the tabulated data. Given the values of two (or one) independent variables, the subroutine performs an interpolation in the directions of independent variables on a table of dependent and independent variables, to obtain the corresponding dependent argument.

Model test

In order to test the validity of the model and the accuracy of the solution of the model equations it is desirable to test the results against solutions obtainable by other analytical means.

Let us consider the case in which the electrolyte system is lumped and the mass of KOH remains constant in the electrolyte cavity. The analytical solution for the change of electrolyte concentration with time as a result of diffusion of water can be obtained as follows.

The rate of mass accumulation of water in the fuel cell equals the rate of mass generation minus the rate of mass evaporated from the electrolyte. If i amperes per unit electrode area per second is drawn from the cell then

$$\dot{m}_{\text{generated}} = \frac{i}{2F} M_2 WZ, \tag{19}$$

where $i/2F$ mol/s cm^2, W is the width and Z is the height of the electrode.

Introducing the definition of the concentration of the KOH in the electrolyte by weight, F_1, the mass balance equation is

$$m_1 \frac{\left(\mathrm{d}\,\frac{1}{F_1}\right)}{\mathrm{d}t} = \left[\frac{9i}{F} - \frac{18 P_{\text{eff}} D_{2\text{-H}}}{\bar{R}T} \cdot \frac{(P_e - P_s)}{t_{g,a}}\right] WZ, \tag{20}$$

where the mass of the potassium hydroxide, m_1, in the electrolyte is constant.

Now, assume that the partial pressure of water vapor in the hydrogen chamber, P_s stays constant and the cell is operating at constant temperature and pressure, then the equilibrium partial pressure of water in the electrolyte is a function of concentration only. The relation between the electrolyte concentration and vapor pressure in logarithmic coordinates at a given temperature is very nearly linear over a certain range and can be expressed by the linear

logarithmic form

$$P_e = e^{(A-F_1)/(0.4343B)}, \tag{21}$$

which can be used to represent the data. For small values of the exponential power this equation can be approximated as

$$P_e = 1 + \frac{A - F_1}{0.4343B}. \tag{22}$$

Then Eq. (20) can be integrated from time equal zero, where $F_1 = F_1°$, to any time, t. At 60°C, the values of the exponential power of the equilibrium partial pressure of water in the electrolyte for 40–45% KOH concentration range varies from −0.0586 to −0.5568. These values are sufficiently small that the linearized form indicated in Eq. (22) can be used, this form will have a maximum error of 5% which occurs at the higher concentration range.

$$P_e = 1 + \frac{0.1266 - F_1}{0.1468}\,\text{kPa}. \tag{23}$$

The resultant changes in concentration of the electrolyte with time for two different partial pressures of the water vapor in the hydrogen gas chamber for a specific cell dimension are plotted in Fig. 6 and are called the analytical solution.

The present model, as discussed earlier, assumes the electrolyte volume to remain constant, which gives rise to a KOH generation or disappearance term. The equations for the model operating isothermally were solved numerically and are presented in Fig. 6. In solving the model equations, the partial pressure of the water vapor in the hydrogen gas chamber is kept constant. In addition, the electrolyte concentration is assumed to be lumped in the y-direction, but the generation term $\rho_1(\partial v/\partial y)$ is retained. Figure 6 indicates a close agreement between the two solutions with differences being in the order of 5%.

It should be noted that in the simplified case for which the analytical results are presented, it is assumed that the mass of KOH remains constant which necessitates a change in volume of electrolyte as the mass of water and, correspondingly, the electrolyte concentration changes. However the model, as discussed previously, assumes the volume of electrolyte remains constant such that the mass of KOH will vary as the electrolyte concentration changes. The inclusion of the volume average velocity terms in the model equations permits determination of this KOH mass increase. The agreement in the two different results suggests that the model effectively predicts concentration changes. These results also indicate that the volume average velocity method correctly accounts for electrolyte concentration changes due to mass changes in KOH. The mass change of KOH as predicted from the model results is indicated in Fig. 7.

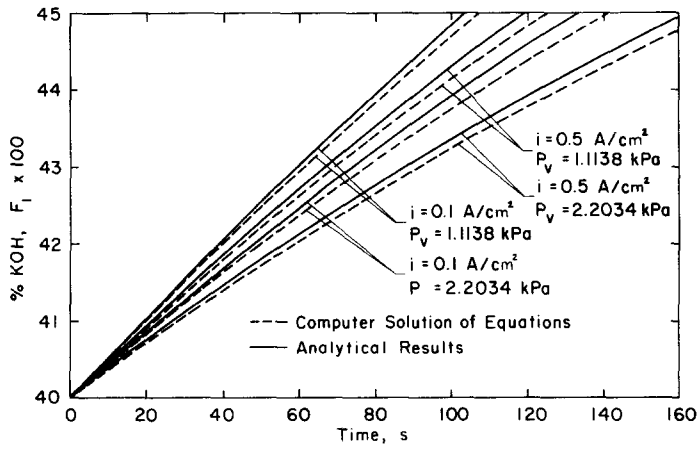

FIG. 6. Change in KOH concentration due to water removal for simplified case.

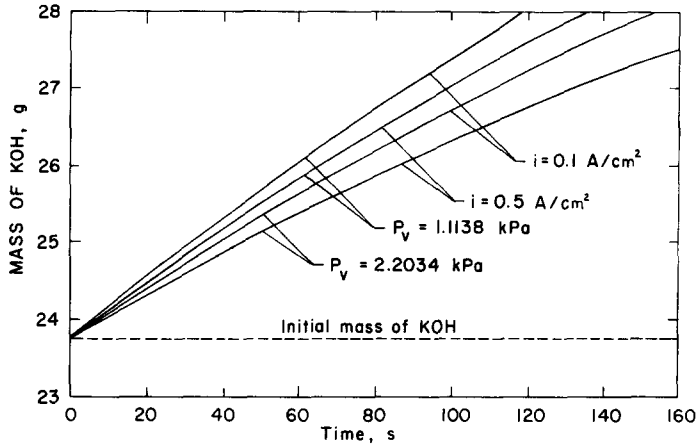

FIG. 7. Change in mass of KOH due to water.

As a second test, a case was considered in which the same cell has a fixed mass of KOH and H_2O and no concentration change due to water gain or loss is assumed and the temperature of the cell varies with time due to heat generation in the cell due to polarization losses and evaporative cooling. Furthermore, it is assumed that the partial pressure of water vapor in the hydrogen chamber, P_s, stays constant and that there is negligible convective heat transfer. For a finite period of time a simplified time dependent exponential function for the polarization is assumed. The resulting closed form solution for the temperature changes of the cell for different partial pressures of water vapor at the hydrogen gas chamber and for different current densities were compared with the computer solution of the model equations, with good agreement [1].

Results of an experimental study of water-rejection dynamics conducted on a matrix type hydrogen–oxygen fuel cell [4] were compared with the prediction based on the model. One comparison was for the cell operated at open circuit, with no water being produced and no heat generated. The transient response of the cell outlet water–vapor flow rate to a step increase in the inlet stream flow rate at the hydrogen chamber agreed with the model transient response. The other comparison was on the transient response of the water–vapor flow rate in the cell outlet stream in the hydrogen chamber when the cell was exposed to a step change in load current for a fixed inlet humidity ratio in the hydrogen chamber. Again the experimental results agreed with model response [1, 2].

RESULTS AND DISCUSSION

The specific dimensions of the fuel cell model considered in both cases are given in Table 1. The nominal values of the initial and inlet parameters corresponding to the working conditions of the cell are given below.

Operating current density, 0.1 A/cm^2
Initial KOH concentration in electrolyte, 30% (by weight)
Initial operating cell temperature, 50°C
Inlet temperature of the hydrogen–water vapor mixture, 50°C
Inlet humidity ratio of the hydrogen–water vapor mixture, 0.70213 gH_2O/gH_2
Inlet mass flow rate of hydrogen, 0.005 g/s
Operating pressure, 101.3 kPa.

In Figs. 8 to 13 any deviations from the above operating conditions are given on the curves. Thus, any parameters not given on these curves assume the above nominal values.

In Fig. 8 the total water evaporated from the electrolyte is given for three different inlet humidity ratios of the hydrogen–water vapor mixture as a function of time. In this figure the humidity ratio, $W_1 = 0.70213$, corresponds to a condition where the partial pressure of the

TABLE 1. Fuel cell dimensions and parameters

The following table lists dimensions and parameters of the fuel cell.	
Fuel cell length	15 cm
Fuel cell width	15 cm
Electrode thickness, $t_{s,a}$	0.05 cm
Gas chamber thickness, t_h	0.2 cm
Distance between anode and cathode, t_e	0.2 cm
Electrode fine pore radius, $r_2(=r_{2,a}=r_{2,c})$	0.1 μm
Electrode fine pore porosity, $P(=P_a=P_c)$	0.8
Effective porosity of the electrodes, $P_{eff}(=P_{eff,a}=P_{eff,c})$	0.5

where a denotes anode and c denotes cathode.

water–vapor mixture equals the water vapor pressure of the electrolyte at 50°C and 30% KOH by weight. Therefore, the value of this relative humidity introduces no driving force for water transport through the electrode as shown by zero slope of the curve at time equals zero. When a load is applied to the fuel cell water is produced and heat is generated resulting in an increase in water concentration and temperature increases the water vapor pressure of the electrolyte. This effect will in turn cause evaporation of water from the electrolyte. Smaller values of humidity ratio ($W_1 < 0.70213$) result in an initial driving force as indicated by the positive slope of the curve corresponding to $W_1 = 0.5$ at time equals zero. Consequently, humidity ratios larger than 0.70213 results in an initial negative driving force. In Fig. 8, let x_1, x_2 and x_3 denote the differences between the water produced and the water evaporated for $W_1 = 0.5$, $W_1 = 0.70213$ and $W_1 = 1$ humidity ratios, respectively. Figure 8 gives the water accumulated in the electrolyte (x_1, x_2 and x_3). When the time reaches 1140 s, the water evaporated and water produced for $W_1 = 0.5$ are equal to each other ($x_1 = 0$), which results in zero accumulation. The temperature

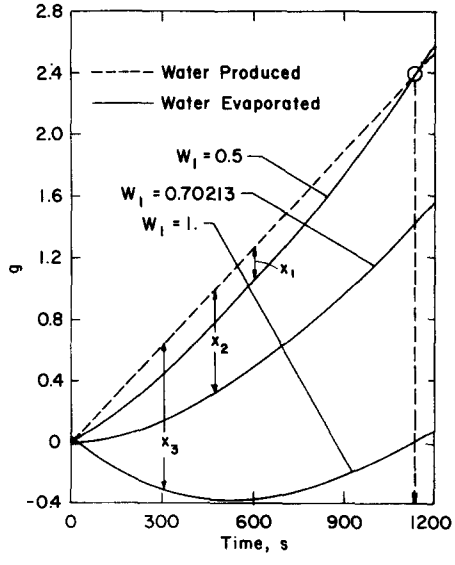

FIG. 8. Water evaporation at different inlet relative humidity ratios.

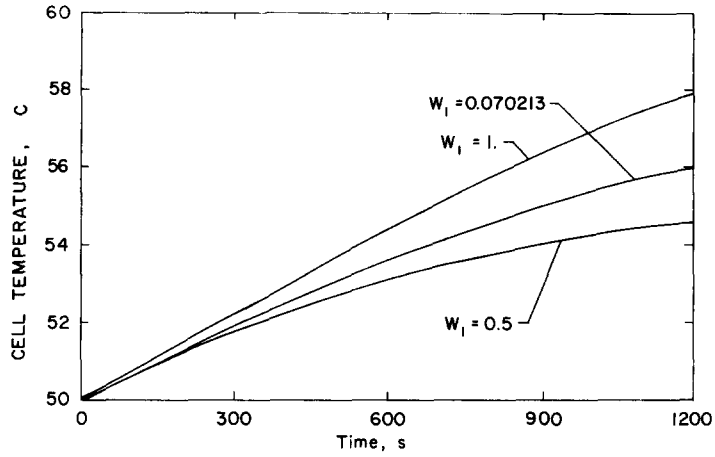

FIG. 9. Effect of inlet relative humidity on the temperature at the top of the cell.

variation associated with Fig. 8 is given in Fig. 9. The temperature at the top of the fuel cell is used because it is the highest temperature observed in the mathematical model. Figure 10 shows the effect of the variation in the operating current density of the cell. The inlet humidity ratio in this curve is kept constant at its nominal value of 0.70213. As the current density increases, the water concentration in the electrolyte and the temperature of the cell increases a resulting increase in the partial pressure of the water vapor in the electrolyte and an increase of the amount of water evaporated from the electrolyte. The maxima in the accumulation of the water in the electrolyte for different values of operating current densities occurs at a time when the water evaporation rate equals the rate of water produced, which is a constant for each current

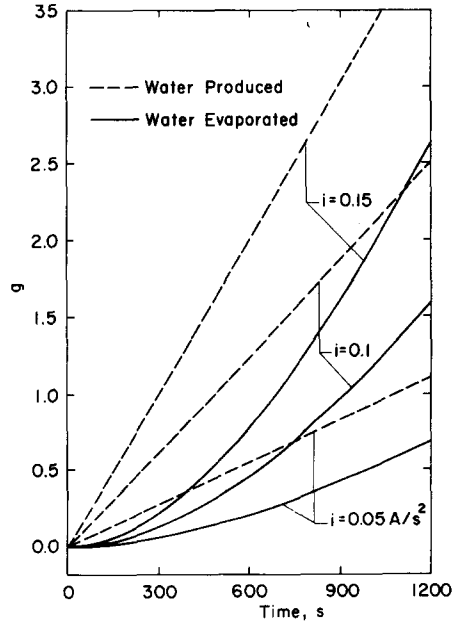

FIG. 10. Water evaporation at different current densities.

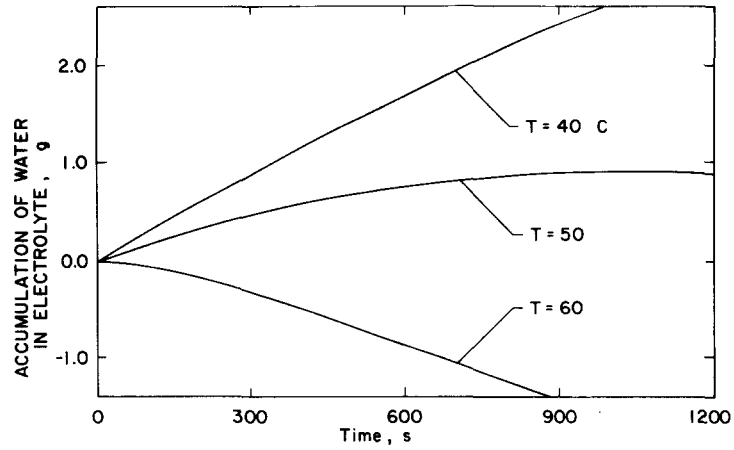

FIG. 11. Effect of initial cell temperature on the accumulation or removal of water from the electrolyte.

density. Figure 11 shows the effects of initial cell temperatures at a current density of 0.1 A/cm^2 and an inlet humidity ratio of 0.70213. As the temperature increases water evaporation rate increases because of the increase in electrolyte vapor pressure with temperature. In all three cases indicated, the inlet hydrogen–water vapor stream is maintained at 50°C.

Figure 12 shows the transient variations in the amount of water accumulated in the electrolyte for different initial electrolyte concentrations. Increasing the initial KOH concentration decreases the partial pressure of water vapor in the electrolyte and therefore decreases the amount of water evaporated. Since the partial pressure of water vapor at 50°C and an electrolyte concentration of 35% KOH (by weight) is less than the partial pressure of water vapor in the hydrogen–water vapor mixture, this causes a decrease in the amount of water accumulated in the electrolyte in order to establish equilibrium. The evaporation is less pronounced at higher KOH concentrations because of the lower water vapor pressure.

Decreasing the flow rate of mixture will decrease the rate of water removal in the reactant gas and therefore increase the accumulation of water in the electrolyte as indicated in Fig. 13. An

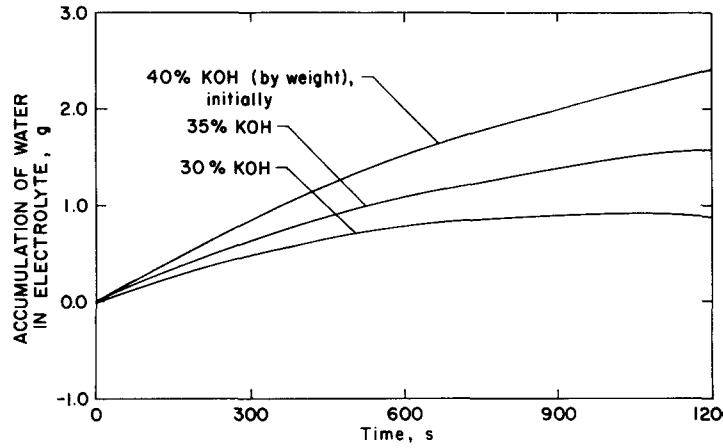

FIG. 12. Effect of initial concentration of electrolyte on accumulation or removal of water from the electrolyte.

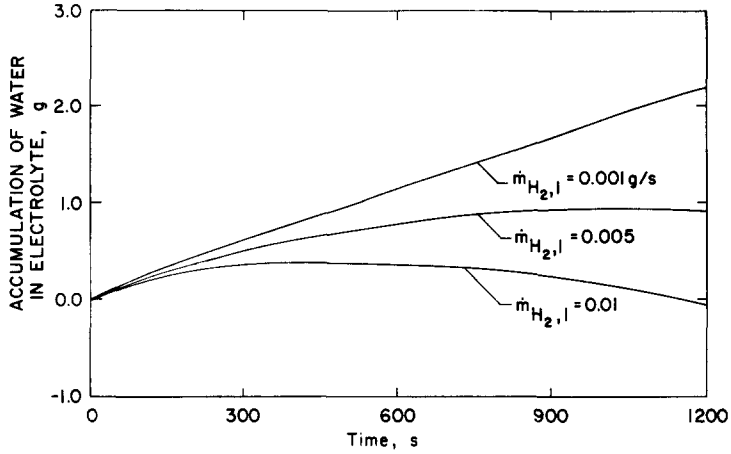

FIG. 13. Effect of mass flow rate of hydrogen on accumulation or removal of water from the electrolyte.

increase in the amount of water evaporated from the electrolyte will cause a decrease in temperature of the fuel cell because of the evaporative cooling effect.

SUMMARY AND CONCLUSIONS

The model proposed in this study couples together the general laws of electrochemical kinetics, mass continuity, diffusive mass transfer and heat transfer in a distributed heat and mass transport analysis, and applies them to a fuel cell model which, unlike the actual case, assumes uniform porosity and complete wetproofing of the electrode structures. The resulting equations to be solved form a complex matrix and require a substantial program for their solution on the digital computer. In spite of these complexities, the resultant simulated model represents the actual fuel cell in a qualitative and quantitative manner such that it can be used in analyzing fuel cell performance and response to changes in operating conditions.

Since the aim in fuel technology is to develop highly reliable, long life, high performance fuel cell systems, the water inventory mechanism should be well understood.

The model and resultant equations presented in this work have been shown to effectively represent transient response characteristics of fuel cells. These equations could be used to parametrically analyze fuel cell response to alterations in operating conditions. Examples of such calculations are presented in Ref. [1].

REFERENCES

1. BAYAZITOGLU, Y., Ph. D. Dissertation, The Univ. of Michigan, Mechanical Engineering Department, Ann Arbor, Michigan.
2. BAYAZITOGLU, Y., SMITH, G. E. & CURL, R. L., Heat and mass transfer analysis of a H_2–O_2 fuel cell, *Hydrogen Energy*, Part B, pp. 859–873, ed. T. N. Veziroglu, Plenum Press, (1975).
3. PROKOPIUS, P. R. & HAGEDORN, N. H., Investigation of the dynamics of water rejection from a hydrogen–oxygen fuel cell to a hydrogen stream, NASA TN D-4201 (1967).
4. PROKOPIUS, P. R. & EASTER, R. W., Mathematical model of water transport in Bacon and alkaline matrix-type hydrogen–oxygen fuel cells, NASA TN D-6609 (1972).
5. MALVERN, L. E., *Introduction to the Mechanics of a Continuous Medium*, p. 168, Prentice-Hall, New Jersey (1969).
6. THAM, N. K., WALKER, R. D., & GUBBINS, K. E., Diffusion of oxygen and hydrogen in aqueous potassium hydroxide solutions, *J. Phys. Chem.* **74,** 1747 (1970).
7. WALKER, R. D., A study of gas solubilities and transport properties in fuel cell electrolytes, NGR 10-005-022 (1968).
8. MCCARTY, K. P. & E. A., Kirkendall effect in gaseous diffusion, *Phys. Fluids*, **3,** 908 (1960).
9. BERGER, C., *Handbook of Fuel Cell Technology*, Prentice-Hall, New Jersey (1968).

10. *International Critical Tables*, Vol. III, p. 373, McGraw-Hill, New York, (1928).
11. ICZKOWSKI, R. P , Mechanism of the hydrogen gas diffusion electrode, *J. Elect. Soc.* **111,** 1072 (1964).
12. BOCKRIS, J. O'M. & SRINIVASAN, S., *Fuel Cells: Their Electrochemistry*, McGraw-Hill, New York (1969).
13. AKERLOF, G. & KEGELES, G., Thermodynamics of concentrated aqueous solution of sodium hydroxide, *J. Chem. Phys.* **62,** 620 (1940).
14. NORRIS, R. H. & STREID, D. D., Laminar-flow heat-transfer coefficients for ducts, *Trans. ASME* **62** (1940).